Inferring physical parameters from images of vibrating carbon nanotubes.

M. M. J. Treacy, A. Krishnan and P. N. Yianilos,

NEC Research Institute, Inc., 4 Independence Way, Princeton, NJ 08540-6685

Abstract

We describe a *hidden parameter inferencing* algorithm for deducing the length, width and vibration profile from images of thermally excited single-wall carbon nanotubes. With accurate estimates of these parameters, the Young's modulus can be deduced. The algorithm is sensitive to shot noise in the image, primarily because of the low nanotube image contrast. Noise causes the nanotube length and width to be overestimated, and the vibration amplitude to be underestimated. After correcting for shot noise, we infer an average value of the Young's modulus of $\langle Y \rangle = 1.20 \pm 0.20$ TPa, which is larger than the currently accepted value for graphite.

Introduction

Carbon nanotubes have interesting physical properties because of their closed, seamless, graphite-based structure (Dresselhaus et al., 1988). Their structural perfection suggests that single-walled nanotubes may have greater strength and stiffness than conventional graphite fibers, which tend to contain structural defects. Furthermore, there are theoretical predictions suggesting that the Young's modulus of the smallest diameter nanotubes, $\leq$ 1 nm, may be significantly greater than that for planar graphite (Cornwell and Wille, 1997); (Hernandez et al., 1998); (Overney et al., 1993); (Robertson et al., 1992); (Yakobson et al., 1996).

Although there is a range of quoted values in the literature, the in-plane Young's modulus of graphite is thought to be around 1×10^{12} Pa (*i.e.* 1 TPa) (Baker and Kelly, 1964); (Blakslee et al., 1970); (Jacobsen et al., 1995); (Seldin and Nezbeda, 1970). Most measurements are made on

pyrolytic graphite, since large single crystals are hard to make. The Young's modulus of individual carbon fibers has been measured by studying their resonant vibration modes when excited by a piezoelectric transducer (Jacobsen et al., 1995). Average values of $\langle Y \rangle = 0.68$ TPa were found. Typical carbon fibers contain many structural imperfections. Consequently, they tend to have a lower effective Young's modulus compared with graphite. However, it is well known that even high quality pyrolytic graphite is not defect-free. Consequently, measurements to-date may still be underestimates of the true Young's modulus of graphite.

Single-walled carbon nanotubes are about 3 orders of magnitude smaller than typical carbon fibers, and thus cannot be manipulated and measured as easily. Treacy *et al.* (Treacy et al., 1996) showed that the Young's modulus of multi-walled nanotubes could be inferred by measuring the thermal vibration amplitude of freestanding nanotubes in the TEM. In that study, they found that $\langle Y \rangle = 1.8 \pm 0.8$ TPa for multi-walled nanotubes. The wide spread in values was attributed mainly to the uncertainty in determining the freestanding length since the true anchor point can not be accurately determined from the 2-dimensional projection of a TEM image. In a follow-up report, Krishnan *et al.* (Krishnan et al., 1998) used a similar technique to estimate the Young's modulus of single-walled nanotubes, and found a value of $Y = 1.25 \pm 0.2$ TPa. In that work, Krishnan *et al.* (Krishnan et al., 1998) developed a *hidden parameter inferencing technique* which improves estimates of the nanotube dimensions and vibration amplitude, thereby obtaining more accurate estimates of the Young's modulus. Poncharal *et al.* (Poncharal et al., 1999) have recently shown that by subjecting multi-walled nanotubes to high frequency AC electric fields, resonant frequencies can be determined by observing the vibration modes in the TEM. They get values of ~1.2 TPa. Although this method allows accurate estimates of the length by observing more than one resonant frequency, resonant frequencies are sensitive to any non-uniformity in mass distribution along the length of the nanotube. In particular, any extraneous mass at the tip will strongly reduce the resonant frequency. Poncharal *et al.* (Poncharal et al., 1999) proposed using this frequency shift to measure very small masses using assumed values for the Young's

modulus. Measurements made by atomic force microscopy on nanotubes draped across holes, or lying on silicon supports, also suggest a value of ~1.0 TPa (Wong et al., 1997).

In this paper, we describe in more detail the *hidden parameter inferencing* technique that was used in our previous report (Krishnan et al., 1998) for extracting the nanotube dimensions and vibration amplitude. In this technique, we use our knowledge of the form of the vibration profile to infer the most likely values of the nanotube freestanding length, its width and vibration amplitude. Performing a least squares fit between the idealized image and the image data optimizes these parameters. This technique is relatively insensitive to microscope imaging conditions, but, because of weak image contrast, is vulnerable to shot noise.

We have presented elsewhere the theory of stochastically vibrating nanotubes (Krishnan et al., 1998). Here we summarize the principle behind the measurement, and present a more detailed description of the hidden parameter inferencing algorithm.

1. Thermal vibrations in freestanding nanotubes

For a freestanding multi-walled nanotube of length L, with inner and outer radii a and b respectively, the mean square lateral thermal vibration amplitude σ^2 at the tip is given by (Krishnan et al., 1998)

$$\sigma^2 = 0.4243 \frac{L^3 kT}{Y\left(b^4 - a^4\right)} \tag{1}$$

Y is the Young's modulus. In the derivation of this formula, it is assumed that the nanotube behaves like a clamped cantilever. The contributions from higher-order vibration harmonics are included. A similar formula describes the vertical tip vibration amplitude. The vertical and lateral motions are independent, and only the lateral motion is directly visible in micrographs. Because the nanotube is a thermally activated stochastic oscillator, the time-averaged motion of the tip $\langle P(y) \rangle$ has a Gaussian probability density (Krishnan et al., 1998)

$$\langle P(y)\rangle = \frac{1}{\sqrt{2\pi}\sigma}\exp\left(-\frac{y^2}{2\sigma^2}\right) \tag{2}$$

Typically, $\sigma \leq 0.5$ nm, and the depth of focus of the objective lens is typically > 5 nm, thus any additional image blurring due to the vertical motion in and out of the focal plane is small. In principle, all the parameters L, a, b and σ can be measured directly off electron micrographs, immediately giving the Young's modulus Y, provided the temperature T is known. However, in practice, the actual clamping point of the nanotube can not be determined accurately, introducing an uncertainty in L. Also, the nanotube itself may not be perfectly horizontal, which means that micrographs will portray a shorter projected length $L(1-\cos\theta)$, where θ is the angle from the horizontal. On average, the nanotube length will be systematically underestimated. It is possible to estimate θ by tilting the nanotube and studying how the projected length changes. Figure 1 shows an example TEM bright field micrograph of a single-walled nanotube vibrating at room temperature. It is not clear where the nanotube is clamped. It can not be assumed that the nanotube is clamped exactly at the point A where it projects past the support. There is also uncertainty in the tip vibration amplitude because we do not have an unambiguous image of the stationary portion of the nanotube near the clamped region to use as a reference. In addition, it is assumed that the nanotube is uniform along its length. This assumption is reasonable for clean single-walled nanotubes.

Equation (1) is valid only in the limit that $b-a >> G$, and is thus not valid for single-walled nanotubes, where $b = a$. For single-walled nanotubes, a more appropriate expression is

$$\sigma^2 = 0.8486\frac{L^3 kT}{YWG\left(W^2+G^2\right)}. \tag{3}$$

Here, W is the width of the single-walled nanotube, and G is a parameter equal to the nominal width of the nanotube wall. We believe that the value $G \approx 0.335\,\text{nm}$, the graphite interplanar spacing, is a reasonable value to adopt.

Our task is to estimate Young's modulus by studying a TEM image of a freestanding, thermally excited, single-wall nanotube. We need to determine L, W, σ as accurately as possible. The root mean square vibration profile $\sigma(x)$ of a clamped nanotube fiber, at position x along its length, is given to a good approximation by (Krishnan et al., 1998)

$$\sigma(x) = \frac{3\sigma(L)}{L^3}\left[\frac{1}{2}Lx^2 - \frac{1}{6}x^3\right]. \qquad (4)$$

$\sigma(L)$ is the root mean square (r.m.s.) vibration amplitude at the tip, $x = L$. The exact expression for the r.m.s. vibration profile is relatively complicated and is computationally expensive; thus equation (4) is the preferred form. As an aside, we note that equation (4) also describes the bending profile of a nanotube that is pushed sideways by a point force at the tip.

2. Hidden parameter inferencing

In principle, the Young's modulus Y, can be estimated from micrographs simply by estimating the freestanding nanotube length L, its width W, and tip vibration amplitude $\sigma(L)$ directly off a micrograph. However, as explained above, there are uncertainties in these values because micrographs present a projection of the nanotube, introducing uncertainty as to the exact location of the clamping point. Exploiting our knowledge of the nanotube vibration profile can significantly reduce this uncertainty. By fitting the cleanest portion of the nanotube image to the functional form in equation (4), we can extract the best set of values, L, $\sigma(L)$ and W, which fit the data.

The algorithm is as follows.

1. Select a clean length of the nanotube image. In the example shown in Figure 1, the clean region is denoted by the tick marks. There is no support material in the background and the nanotube does not have any obvious detritus attached to it. The tip itself is excluded from the selection since its structure is different from the shaft of the nanotube.

2. Rotate the selection so that the axis of the nanotube is either along x or y. We shall assume x. To minimize corruption of the image data, we first expand the image by a factor of 4 in each direction using a bi-cubic interpolation algorithm. Then the image is rotated. Finally, the image is reduced by a factor of 4 back to its original scale. A good test for data corruption is to reverse the process and compare the doubly rotated image with the original data. In our case, we found that there was negligible difference. The rotated, clipped region for the nanotube in Figure 1, is shown in Figure 3a.
3. We make a first guess as to the image intensity profile $I_0(y)$ at the stationary end (at $x = 0$) of the nanotube. In all likelihood, the clamped $x = 0$ portion of the nanotube will not be included in the selected portion of the nanotube image. A good first guess as to $I_0(y)$ is obtained by averaging the nanotube intensity profile along y at the end nearer the clamping point.
4. Using this approximation to $I_0(y)$, we compute an image for candidate values of $\sigma(L)$ and L. The image data that we are trying to match is assumed to be a section of the nanotube located between the points $x = x_0$ and $x = x_1$, where $0 \le x_0, x_1 \le L$. The difference $L - x_1$ represents the length of the excluded tip region. This is usually short and can be estimated directly from the micrograph. Our unknown parameters are, therefore, x_0 and $\sigma(L)$. The model image intensity profile $I_x(y)$ is determined by systematically smearing the stationary profile $I_0(y)$ as a function of x between $x_0 \le x \le x_1$. Thus,

$$I_x(y) \equiv \left[I_0(y) \otimes \frac{1}{\sqrt{2\pi}\sigma(x)} \exp\left(-\frac{x^2}{2\sigma^2(x)} \right) \right]_{x_0}^{x_1}. \qquad (5)$$

5. The model image and the actual image are compared by subtracting one from the other and summing the squares of the differences in pixel intensities. This sum provides a goodness of fit. The goal is to minimize this difference by adjusting the assumed

profile $I_0(y)$. We found that Powell's method was an efficient algorithm for doing this (Press et al., 1992).

6. Once the best fit has been determined, we then carry out a systematic dense grid search over a wide range of values x_0 and $\sigma(L)$ in search of the global best values. Once we have x_0, we know L and the best profile $y(0)$. From $y(0)$ we get the best estimate of the width W of the stationary nanotube. These best-fit values, L, $\sigma(L)$ and W, are inserted into equation (3) to yield a best-fit estimate of the Young's modulus.

W was estimated by comparing the profile $y(0)$ with multislice image simulations computed by the MacTempas (Kilaas, 1988). Models of comparable diameter to the three nanotubes studied here (W = 1.0 – 1.5 nm) were generated, and through-focal series of images were simulated. For images close to the Scherzer focus, the darkest image features were found to correspond closely to the outer walls of the nanotube. Thus, in our best-fit profile $y(0)$, the distance between the two lowest intensity features was then equated with W. Unlike the estimates of L and $\sigma(L)$, the estimate of W is subjective. We estimate the accuracy of W to be better than ±5%.

The computed best fit for the data is shown in Figure 3b. The full length (x = 0 to L) of the best-fit image $I_x(y)$ is inserted into Figure 1, rotated so as to be parallel to the original image. The best-fit length is about 40% longer than the length projecting beyond the edge of the support, point A in Figure 1.

Results and discussion.

It is rare to find clean, isolated, single-wall nanotubes of the right length. Frequently, nanotubes are part of larger rope bundles, or when isolated, are covered with small particles (presumably carbon detritus) (Dujardin et al., 1998); (Guo et al., 1995); (Thess et al., 1996). Frequently, isolated nanotubes are either too long, so that the free ends flail and twitch erratically, or they are so short that the vibration at the free end is undetectable. Optimal single-walled nanotubes are in the length range 10 nm ≤ L ≤ 100 nm. Three such nanotubes were

imaged using a Hitachi H9000 NAR operated at 100 kV. The lower accelerating voltage was used to increase image contrast and to reduce beam damage. Bright field images were collected using a Gatan model 690 slow-scan CCD camera, and processed using Digital Micrograph v2.5 software. Samples were imaged at room temperature at a magnification of ×180,000 at a nominal dose rate of ~800 electrons.sec^{-1}.nm^{-2}. Graphite lattice fringes were used to calibrate the microscope magnification. Typically, exposure times were adjusted to collect ~1000 counts per pixel. Frequently, a second or third image of the same nanotube would be recorded to check for any undesirable variations in the image with time, such as drift or a tilting of the nanotube. Each nanotube received a total dose of about 20,000 electrons.nm^{-2} during the experiment, and there was no obvious degradation.

The images of the three single-wall nanotubes were analyzed by our hidden parameter inferencing method. These three nanotubes were chosen out of about 60 candidates because they were isolated, clean, and did not flinch under the electron beam – implying that they were firmly anchored and defect-free. The least squares fit yielded for these nanotubes the values shown in Table 1.

An indication of the robustness of the hidden parameter inferencing algorithm can be obtained by viewing the contour plot of the least square differences between simulated and data images for the search grid of L and $\sigma(L)$ values. Figure 2 is the contour plot for the refinement of nanotube 1. The contours reveal a "valley" aligned approximately parallel to the L axis. The minimum value is located at L = 36.8 nm, $\sigma(L)$ = 0.33 nm. The first contour corresponds to an increment in the least square difference of only ~0.15%. Thus this "valley" is more like a shallow dimple. It appears from the relative shallowness of the contours along the L axis that the length estimate is more vulnerable to error than the $\sigma(L)$ estimate.

For a clean nanotube, shot noise in the image is the largest contribution to the least square difference between the computed image and data.

Figure 3 explores the impact of shot noise on the image of nanotube 1. Figure 3a shows the original image data taken from Figure 1. Figure 3b is the best-fit simulation. The noise in the

original data is mostly shot noise, as deduced from the mean square difference per pixel between the two images. Shot noise makes the walls of the nanotube appear rough, as can be confirmed by adding noise to the smoothed best-fit simulation. Figures 3c, 3d and 3e show the best fit simulation of Figure 3b with noise added, at signal-to-noise values of about 10, 5 and 1 respectively. The original data has an estimated signal-to-noise of around 1.3.

It is clear that increased noise acts to roughen the nanotube image. We need to define a consistent measure of the noise. The contrast of the nanotube 1 image is around 4%, that is, $C \approx$ 40 counts out of 1000. This is the signal. For a perfect CCD detector, the standard deviation of the shot noise should be about $N^{1/2}$, where N is the average number of counts per pixel. Thus, for $N = 1000$, $N^{1/2} \approx 30$. However, the measured standard deviation with the specimen removed is ~7.5 counts per pixel, about one quarter of the ideal value. This apparent reduction in noise seems to be caused by imperfect transfer of contrast by the CCD detector due to leakage of signal to adjacent pixels. The noise simulations of Figures 3c, 3d and 3e take into account this contrast transfer characteristic. For convenience, the signal-to-noise we refer to here is $C / N^{1/2}$.

The impact of this shot-noise induced image roughness on the best-fit L and $\sigma(L)$ values was investigated. Table 2 shows how $L, \sigma(L)$ and Y change as a function of noise.

From Table 2, it is clear that decreased signal-to-noise tends to increase systematically the estimated length and width of the nanotube, but with a concomitant decrease of the tip vibration amplitude. The apparent lengthening occurs because noise interferes with the detection of curvature in the nanotube vibration profile as a function of axial position x. Noise tends to make the vibration profile appear linear with position x. The tip region of a vibrating nanotube has the least bending curvature. Thus, with increasing noise, the data appears to be taken from near the tip of a longer, broader, nanotube that is vibrating with smaller amplitude. The Young's modulus depends on these values as $Y \propto L^3/W^3\sigma^2(L)$, for $W >>$ 0.335 nm. From the Table, we see that the systematic errors in L, W and $\sigma(L)$ tend to cancel. Thus, for signal-to-noise values of 2 or more, the error in the inferred Young's modulus is small relative to the errors in L, W and $\sigma(L)$. For the simulated signal-to-noise of 1.3, corresponding to the conditions under which our data

were collected, Table 2 suggests that we have overestimated the Young's modulus by about 5%. With very noisy images, there is little difference detected in the intensity profiles from either end, thus the nanotube appears increasingly to be stationary and straight, and hence stiffer.

This noise correction suggests that the single-walled nanotubes have a Young's modulus of around 1.20 ± 0.2 TPa, which is consistent with the value for graphite, 1.06 TPa.

Poncharal *et al.* (Poncharal et al., 1999) and Osakabe *et al.* (Osakabe et al., 1997) have estimated Young's modulus of fibers by measuring the natural vibration frequency modes. By exciting the first two (or more) harmonics with high frequency radiation, the clamped length of the fiber is readily estimated without having to guess the anchor point. However, the frequency measurement method is likely to be sensitive to particulate contaminants that lie on the nanotube. Contaminants will tend to weigh down the nanotube and depress the vibration frequency (Poncharal et al., 1999). Contaminants will not have a large impact on the vibration amplitude, unless they also happen to weaken the nanotube at the contact point.

It seems that an optimal microscopy method would be to use the induced harmonics to estimate the clamped length, and to use the least-square image optimization to infer the best-fit vibration profile. This approach will probably yield a more reliable clamped length estimate L than that obtained by the least-squares image optimization alone. In the absence of specimen drift, the accuracy of the vibration profile will undoubtedly improve if the image exposure time is increased in order to enhance the signal-to-noise. When optimizing the vibration profile of a dirty nanotube, those sections of the image containing contaminants should be masked so that they do not corrupt the optimization.

Currently, the hidden parameter inferencing method described here has an accuracy of around ±20% for Young's modulus measurements. It is not too far-fetched that, with careful experimentation, hidden parameter inferencing methods are capable of accuracy closer to ±5%. With this level of accuracy, any dependency of Young's modulus on nanotube diameter or helicity may eventually be elucidated.

Acknowledgments.

The authors wish to thank Erik Dujardin, Thomas Ebbesen and Murray Gibson for many useful discussions.

Figure captions.

Figure 1: Single-walled nanotube 1. Thermal vibrations are evident by the slight blurring of the tip relative to the base. Point A indicates a good starting guess for the anchor point of the nanotube. However, the least squares best-fit image, inserted to the left, shows that the true anchor point, 0, extends well into the support.

Figure 2: Contour plot showing the least square differences between simulated and data images for a grid of L and $\sigma(L)$ values. The lowest contour level occurs at L = 36.8 nm, $\sigma(L)$ = 0.33 nm, which is taken to be the best overall fit. This point corresponds to a least square difference per pixel of ~1000, which is consistent with the average signal-to-noise in the original image. The contours are spaced by a least squares difference of around 1.5%.

Figure 3: a) Original clipped image of nanotube 1, taken from Figure 1 and rotated. This is the image data set that was fit by the hidden parameter inferencing algorithm. b) Best-fit simulation with L = 36.8 nm, $\sigma(L)$ = 0.33 nm. c) - e) Best-fit image with simulated noise added, with signal-to-noise values of 10, 5 and 1 respectively.

References

Baker C, Kelly A (1964) The effect of neutron irradiation on the elastic moduli of graphite single crystals. *Philos Mag* 9: 927

Blakslee OL, Proctor DG, Selden EJ, Spence GB, Weng T (1970) Elastic constants of compression-annealed pyrolytic graphite. *J Appl Phys* 41: 3373-3382

Cornwell CF, Wille LT (1997) Elastic properties of single-walled carbon nanotubes in compression. *Solid State Commun* 101: 555

Dresselhaus MS, Dresselhaus G, Sugihara K, Spain IL, Goldberg HA (1988) Graphite Fibers and Filaments. New York, Springer-Verlag.

Dujardin E, Ebbesen TW, Krishnan A, Treacy MMJ (1998) Purification of single-shell nanotubes. *Advanced Materials* 10: 611-613

Guo T, Nikolaev P, Thess A, Colbert DT, Smalley RE (1995) Catalytic growth of single-walled nanotubes by laser vaporization. *Chem Phys Letts* 243: 49-54

Hernandez E, Goze C, Bernier P, Rubio A (1998) Elastic Properties of C and $B_XC_YN_Z$ Composite Nanotubes. *Physical Review Letters* 80: 4502

Jacobsen RL, Tritt TM, Guth JR, Ehrlich AC, Gillespie DJ (1995) Mechanical properties of vapor-grown carbon fiber. *Carbon* 33: 1217-1221

Kilaas R (1988). Macintosh program for simulation of High resolution TEM Images. Lawrence Berkeley Laboratories. Berkeley, Berkeley.

Krishnan A, Dujardin E, Ebbesen TW, Yianilos PN, Treacy MMJ (1998) Young's modulus of single-walled nanotubes. *Phys Rev B* 58: 14013-14019

Osakabe N, Harada K, Lutwyche MI, Kasai H, Tonomura A (1997) Time-resolved observation of thermal oscillations by transmission electron microscopy. *Appl Phys Lett* 70: 940

Overney G, Zhong W, Tomanek D (1993) Structural rigidity and low frequency vibrational modes of long carbon tubules. *Zeit Physik* D 27: 93

Poncharal P, Wang ZL, Ugarte D, Heer WAd (1999) Electrostatic deflections and electromechanical resonances of carbon nanotubes. *Science* 283: 1513

Press WH, Teukolsky SA, Vetterling WT, Flannery BP (1992) Numerical Recipes in C. Cambridge, Cambridge University Press.

Robertson DH, Brenner DW, Mintmire JW (1992) Energetics of nanoscale graphitic tubules. *Phys Rev B* B 45: 12592-12595

Seldin EJ, Nezbeda CW (1970) Elastic constants and electron-microscope observations of neutron-irradiated compression annealed pyrolytic and single-crystal graphite. *J Appl Phys* 41: 3389-3400

Thess A, Lee R, Nikolaev P, Dai H, Petit P, Robert J, Xu C, Y. H. Lee, Kim SG, Rinzler AG, et al. (1996) Crystalline ropes of metallic carbon nanotubes. *Science* 273: 483

Treacy MMJ, Ebbesen TW, Gibson JM (1996) Exceptionally high Young's modulus observed for individual carbon nanotubes. *Nature* 381: 678

Wong EW, Sheehan PE, Leiber CM (1997) Nanobeam Mechanics: Elasticity, Strength, and Toughness of Nanorods and Nanotubes. *Science* 277: 1971-1975

Yakobson BI, Brabec CJ, Bernholc J (1996) Nanomechanics of carbon tubes: Instabilities beyond linear response. *Phys Rev Letts* 76: 2511

	L (nm)	$\sigma(L)$ (nm)	W (nm)	Y (TPa)
Nanotube 1	36.8	0.33	1.50	1.33
Nanotube 2	24.3	0.18	1.52	1.20
Nanotube 3	23.4	0.30	1.12	1.02

Table 1: Inferred physical parameters for three optimal single-wall nanotubes.

Signal-to-noise	L (nm)	$\sigma(L)$ (nm)	W (nm)	Y (TPa)
∞	36.8	0.33	1.50	1.33
10	40.0	0.33	1.6	1.31
5	38.6	0.32	1.6	1.29
1.3	40.1	0.315	1.65	1.40
1	41.3	0.31	1.70	1.47

Table 2: Effect of shot noise on the inferred physical parameters.

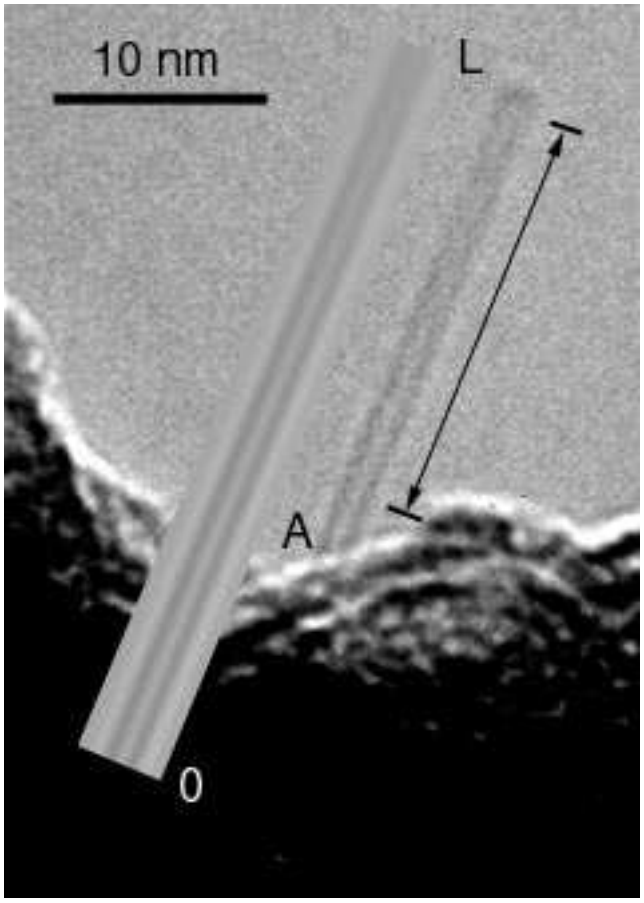

Figure 1